Received April 23, 2019, accepted May 9, 2019, date of publication May 13, 2019, date of current version May 28, 2019.

Digital Object Identifier 10.1109/ACCESS.2019.2916464

Optimal Maneuver Trajectory for Hypersonic Missiles in Dive Phase Using Inverted Flight

SHILI TAN[1], HUMIN LEI[1], AND TAO LIU[2]
[1]Air and Missile Defense College, Air Force Engineering University, Xi'an 710051, China
[2]China Aerodynamic Research and Development Centre, Mianyang 621000, China

Corresponding author: Shili Tan (tanslchn@163.com)

This work was supported by the National Natural Science Foundation of China under Grant 61703421, Grant 61773398, and Grant 61873278.

ABSTRACT To determine the optimal trajectory for the dive phase of a hypersonic missile, a maneuver strategy using inverted flight is presented. The combat scene that the hypersonic missile attacks the fixed target on the ground is considered in this paper. Particularly, a maneuvering form named inverted flight is first applied to the hypersonic missiles. Afterward, an optimal trajectory is designed by minimizing the attack time with a preset terminal flight path angle, where the constraints of the angle of attack, dynamic pressure, heating transfer rate, and normal overload are taken into account. In order to solve the designed trajectory optimization problem, an improved hp-adaptive pseudospectral method with mesh size reduction is presented. The simulation results show that the proposed algorithm can significantly reduce the mesh scale with satisfactory accuracy and the trajectory obtained by the proposed algorithm is in accordance with the actual flight law. Furthermore, contrast simulation demonstrates that the inverted flight has better trajectory performance than normal flight.

INDEX TERMS Trajectory optimization, hypersonic missile, inverted flight, pseudospectral method, mesh refinement.

I. INTRODUCTION

The hypersonic vehicles are mainly divided into three typical categories: reentry gliding, air-breathing cruise, and rocket-powered aerospace transport [1]. As for the hypersonic missiles, reentry gliding and air-breathing cruise are usually adopted. The hypersonic missiles powered by the scramjet or the booster rocket have become the latest global strike weapons [2]. As the terminal of the whole manruver process, the flight in dive phase directly determines whether the strike mission can be completed [3]. For the sake of achieving better flight performance, some researchers have made active attempts. To avoid ablation of aerodynamic rudders under harsh heating condition, a control mechanism named moving mass control (MMS) has been designed for the reentry vehicles [4]. And, a novel configuration of internal mass moving is proposed for bank-to-turn (BTT) control in details [5]. In addition, a higher order sliding mode (HOSM) disturbance observer and double-layer gain-adaptation algorithm are proposed to deal with the matched and unmatched disturbances [6]. Further, the finite- and fixed-time nonrecursive HOSM observer is studied, achieving a better performance than the finite-time recursive HOSM differentiatorb [7]. Recently, researchers have been paying more attention to the design of the controller with high precision and strong robustness. However, few studies have been conducted on the trajectory optimization of the hypersonic missiles in dive phase. The combat scene that the hypersonic missile attacks the fixed target on the ground is considered in this paper. We aim to design an optimal maneuver trajectory to break through enemy's air defense system and maximize target penetration.

The maneuvering form for the hypersonic missile in dive phase is first discussed. Mehta *et al*. established the longitudinal model of the hypersonic missile and generated the optimal trajectory by incorporating the terminal conditions to achieve the maximum target penetration [8]. Based on this research, a HOSM controller is proposed to achieve the tracking of the optimal trajectory with robustness and high accuracy [9]. In addition, Zhu *et al*. simplified the model of the hypersonic missiles by feedback linearization, and then obtained a three-dimensional maneuvering trajectory based

The associate editor coordinating the review of this manuscript and approving it for publication was Chaoyong Li.

on the optimal control theory [10]. Furthermore, the motion camouflage theory is used to obtain the interception condition of the missile and a guidance law is proposed for attacking ground target [11]. It should be noted that the above studies are carried out on the premise of using normal flight and the importance of selecting a suitable maneuvering form has been ignored. Different from the traditional ballistic missiles, the hypersonic missiles are usually designed to be plane-symmetrical in geometry with a high lift-to-drag ratio [12]. Thus, the maneuvering form has an important influence on the trajectory performance. For example, there is a great difference between the trajectory obtained by normal flight and that obtained by inverted flight. In order to take the unique aerodynamic shape of the hypersonic missiles into account, two typical maneuvering forms, i.e., the normal flight and the inverted flight, are studied in this paper.

As for how to solve the trajectory optimization problem, there are two main types of methods, i.e., indirect method and direct method. Constrained by the dynamic pressure, heating transfer rate, and normal overload, the hypersonic missiles in dive phase have a narrower flight corridor. By the indirect methods, the design process of optimal trajectory will become complex if one considers the path constraints. To meet this challenge, Wang *et al*. converted the constraint of the nominal overload into the constraints of the Euler angles, and then obtained the trajectory by zeroing the line-of-sight(LOS) angular rate [13]. One disadvantage of the above study is that only the constraint of nominal overload is considered, and another disadvantage is that the trajectory obtained by zeroing the LOS angular rate is relatively straight, resulting in the poor ability of target penetration. In order to avoid the troublesome derivation of analytical expressions, the direct method is widely used to solve the problem of trajectory optimization. By discretizing and parametrizing the states and controls, the continuous-time optimal control problem is transformed into a problem of nonlinear programming (NLP) with finite dimensions. The key problem is to design an algorithm with high accuracy and fast convergence. Recently, many studies have focused on the design of algorithms for solving NLP. In [14], a genetic algorithm (GA) is introduced to obtain the optimal trajectory for the hypersonic vehicles in unpowered-gliding phase and the problem of sensitivity to initial value in indirect method is solved. Similarly, GA is used for the trajectory generation of the boost-gliding hypersonic vehicles to maximize the range [15]. In order to improve the accuracy and reduce the computational burden, a semi-analytical algorithm is proposed and its performance has been shown to be significantly superior to GA [16]. In addition, a pattern search algorithm (PS) is designed for the trajectory optimization of the hypersonic boost glide vehicles in [17]. The ratio of lift to drag (L/D) is selected as the control parameter of PS and it is proved that the PS is more efficient than GA. Moreover, the particle swarm optimization algorithm (PSO) is used for the ascent phase trajectory optimization of vehicles with multi-combined cycle engine [18] and reentry phase trajectory optimization of hypersonic weapons [19], with the advantage of good convergence and strong robustness [20].

A direct method, namely, the Gauss pseudospectral method [21] (GPM), has been widely used in the solution of the trajectory optimization problems. For example, for the reentry phase of the hypersonic vehicles [22], the midcourse of the hypersonic interceptions [23], and the ascent phase of the ramjet-powered vehicles [24], the optimal trajectories are all obtained by introducing the GPM. Moreover, the trajectory optimization for the supersonic vehicle with a Turbine-Based-Combined Cycle engine is also solved via the GPM [25]. Compared with other direct methods, the advantage of GPM is that the Karesh Kuhn Tucker (KKT) conditions of transformed NLP are consistent with the first-order optimality conditions of the continuous-time optimal control problem [26]. Furthermore, GPM has global optimality and shows promise in dealing with the complex problems. Thus, GPM is a good choice to solve the trajectory optimization problem considered in this paper. In order to get a better performance, it is necessary to improve the GPM. In [27], a ph mesh refinement method is presented to reduce the computation burden while ensuring the accuracy. Based on the *hp*-adaptive pseudospectral method [27], the optimal trajectory of a spaceplane in the reentry phase is obtained to complete a temporary reconnaissance mission [28].The shortcoming of the ph mesh refinement method [27] is that the mesh can only increase in size, resulting in an increased computational burden. In order to further optimize the algorithm, the adaptive mesh refinement methods with mesh size reduction are studied [29]. In the previous study, we had put efforts into the design of the mesh refinement algorithm [30]. Thus, the improved *hp*-adaptive pseudospectral method is introduced to solve the problem of the trajectory optimization for the hypersonic missiles in dive phase.

Motivated by the above literatures, an optimal maneuver trajectory for the hypersonic missiles in dive phase is presented based on an improved *hp*-adaptive pseudospectral method. First, the model for the hypersonic missile is established wherein the realistic and complete aerodynamic data, published by NASA [31], is adopted. Then, the maneuvering form of the hypersonic missile is discussed. It should be noted that target penetration is negatively correlated with the value of AoO (the inertial angle of obliquity (AoO) is defined as the angle between the normal to the target surface and the missile trajectory [8]). Particularly, a maneuver strategy under inverted flight is adopted in this paper. The inverted flight can make full use of lift to change the direction of velocity, thus achieving the fast strike with a larger flight path angle (i.e. a smaller AoO). Afterwards, an optimal maneuver trajectory is designed by minimizing the attack time with a preset terminal flight path angle, where the constraints of angle of attack, dynamic pressure, heating rate and normal overload are taken into account. Furthermore, a algorithm is presented for the solution of the designed trajectory optimization problem, based on the improved *hp*-adaptive pseudospectral method.

The main contributions of this paper are as follows:

i) An optimal maneuver trajectory is designed by minimizing the attack time with a preset terminal flight path angle. Particularly, the inverted flight is selected as the maneuvering form.

ii) An improved *hp*-adaptive pseudospectral method with mesh size reduction is presented for the solution of the designed trajectory optimization problem.

The rest of this paper is organized as follows. In the next section, the model of the hypersonic missile is given, and an optimal maneuver trajectory using inverted flight is described. The third section gives the algorithm for the solution of the designed maneuver trajectory in detail. Numerical simulation and the conclusion are presented in fourth and fifth sections, respectively.

II. MODELING AND TRAJECTORY OPTIMIZATION DESCRIPTION

A. HYPERSONIC MISSILE MODEL

Ignoring the earth's rotation and assuming that the earth is a sphere [32], the kinematical and dynamic equations of the hypersonic missiles in the ground coordinate system are described as follows [33].

$$\dot{x} = V\cos\gamma\cos\psi \tag{1}$$

$$\dot{h} = V\sin\gamma \tag{2}$$

$$\dot{z} = -V\cos\gamma\sin\psi \tag{3}$$

$$\dot{V} = \frac{-D}{m} - g\sin\gamma \tag{4}$$

$$\dot{\gamma} = \frac{L\cos\sigma - N\sin\sigma}{mV} - \frac{g}{V}\cos\gamma \tag{5}$$

$$\dot{\psi} = -\frac{L\sin\sigma + N\cos\sigma}{mV\cos\gamma} \tag{6}$$

where x, h, and z are the components of the position vector of the hypersonic missile. V, γ, and ψ denote the velocity, flight path angle, and heading angle, respectively. σ is the bank angle. m is the vehicle mass, and g is the gravitational acceleration. The lift L, drag D, and side force N are given as

$$\begin{cases} L = qSC_L \\ D = qSC_D \\ N = qSC_N \\ q = \dfrac{1}{2}\rho V^2, \quad \rho = \rho_0 \exp\left(\dfrac{h_0 - h}{h_s}\right) \end{cases} \tag{7}$$

where q denotes the dynamic pressure, and S is the reference area. ρ is the air density, and ρ_0, h_0, h_s are the constant parameters of atmosphere model [34]. C_L, C_D, and C_N denote the lift coefficient, drag coefficient, and side force coefficient, respectively.

The aerodynamic model used in this paper is derived from the actual data published by NASA [31]. Compared with the methods of nonlinear curve fitting in [35], [36], smaller residual between the fitting curve and the actual data is obtained by using the least square error criterion and quasi-Newton

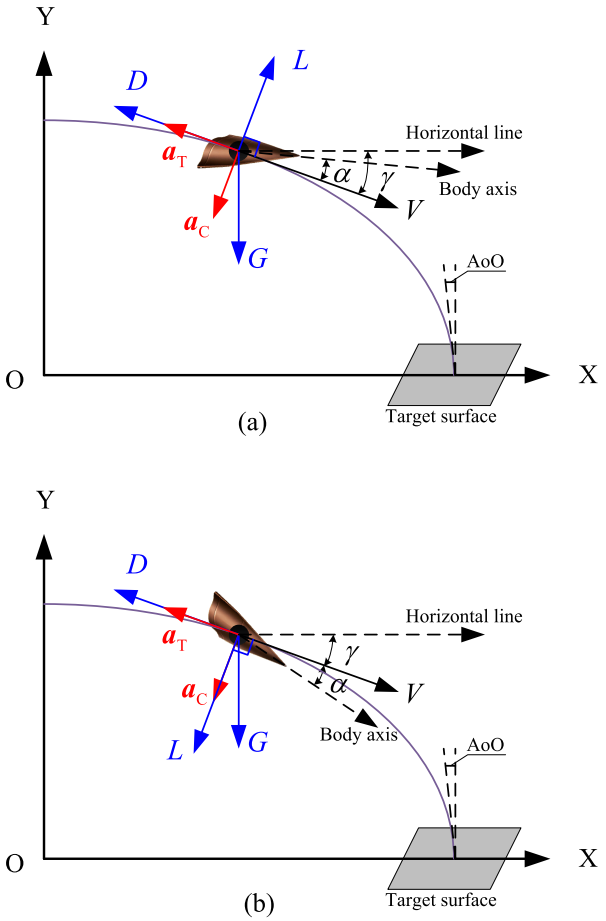

FIGURE 1. Schematic diagrams of force analysis under two maneuvering form. (a) using normal flight. (b) using inverted flight.

modified method in [33]. Thus, the curve fitting model (CFM) described in [33] is adopted in this paper. The expressions of C_L, C_D and C_N are given in the Appendix.

B. TRAJECTORY OPTIMIZATION DESCRIPTION

The combat scene that the hypersonic missile attack the fixed target on the ground is considered in this paper. As the last period of the entire strike mission, the trajectory generation in dive phase is critical to a successful strike mission because it directly determines whether the hypersonic missile can break through the air defense system and cause effective damage to the target. The hypersonic missiles break through the enemy's air defense system relying on the advantage of speed, so the lateral maneuvering is not considered. First of all, two typical maneuvering forms, i.e., the normal flight and the inverted flight, are studied. The schematic diagrams of force analysis under two maneuvering form are given as Fig. 1.

By analyzing the forces of the missile, the centripetal acceleration a_C and the tangential acceleration a_T are given as follows.

$$a_C = \frac{G\cos\gamma \pm L}{m} \tag{8}$$

$$a_T = \frac{D - G\sin\gamma}{m} \tag{9}$$

where $G = mg$ denotes the gravity. The symbol "$\pm$" is selected as "$-$" for the normal flight or as "$+$" for the inverted flight.

In order to narrow the response time of the air defense system, the shortest attack time is needed. The shorter the flight time, the less the kinetic energy loss. Thus, the tangential acceleration a_T is expected to be small enough to remain the velocity a big value. Furthermore, the centripetal acceleration a_C is expected to be big enough to provide a smaller AoO, enhancing the damage ability to the target,. It can be concluded that the larger the value of a_C/a_T is, the more beneficial it is for the dive flight, without considering the constraints.

For the normal flight, the attack of angle (AoA) has to be negative to provide a negative lift if a big value of a_C is wanted. At this time, the design of the control system will become difficult. By using the inverted flight, the above troubles will be avoided. Moreover, the characteristic of L/D under inverted flight is better than those under normal flight, which will provide a bigger value of a_C/a_T. Thus, the inverted flight has more advantages for the hypersonic missile in dive phase.

The maneuver trajectory objective is selected by minimizing the cost functional

$$J = \phi(\mathbf{X}(t_0), t_0, \mathbf{X}(t_f), t_f) = t_f \tag{10}$$

subject to the dynamic constraint

$$\dot{\mathbf{X}} = \boldsymbol{f}(\mathbf{X}(t), \quad \boldsymbol{u}(t), (t) \tag{11}$$

the terminal state constraint

$$\boldsymbol{\phi} = [x - x_f, h - h_f, z - z_f, \gamma - \gamma_f]^T = 0 \tag{12}$$

the control constraints

$$\alpha_{\min} \le \alpha \le \alpha_{\max}, \quad \beta = 0 \tag{13}$$

and the constraints

$$q \le q_{\max} \tag{14}$$

$$\begin{cases} Q_{rate} = C\rho^{0.5}V^{3.07}q_\alpha \le \{Q_{rate}\}_{\max} \\ q_\alpha = h_0 + h_1\alpha + h_2\alpha^2 + h_3\alpha^3 \end{cases} \tag{15}$$

$$\left|n_y\right| = |(L\cos\alpha + D\sin\alpha)/(mg)| \le \{n_y\}_{\max} \tag{16}$$

where the states $\mathbf{X}(t) = [x, h, z, V, \gamma, \psi]^T$, and the inputs $\boldsymbol{u}(t) = [\alpha, \beta, \sigma]^T$. J is the index criterion, and the subscript f denotes the final value of the variables. Eq. (11) is derived from Eqs. (1)$\sim$(6). Q_{rate} is the heating transfer rate, and n_y is the normal overload of the missile. The parameters in Eq. (15) are given as follows [23], [37]: $C = 9.289 \times 10^{-9} BTU \cdot s^{2.07}/(ft^{4.07} \cdot slug^{0.5})$, $h_0 = 1.067$, $h_1 = -1.101$, $h_2 = 0.6988$, $h_3 = -0.1903$.

III. DESIGN OF THE ALGORITHM

In this section, an improved *hp*-adaptive pseudospectral method is introduced to solve the trajectory optimization problem described as Eqs. (10)$\sim$(16). Firstly, the trajectory optimization problem is transformed to the discrete bolza optimal control problem in a mesh M. Then, a mesh refinement method is designed to solve the transformed NLP problem. Different from the traditional *hp*-adaptive pseudospectral method, the mesh scale can be reduced by reducing the number of collocation points and merging adjacent mesh intervals. Finally, the algorithm for solving the trajectory optimization problem is summarized.

A. BOLZA OPTIMAL CONTROL PROBLEM

The trajectory optimization for the hypersonic missiles in dive phase is a non-smooth optimization problem under multiple constraints. If we adopt the indirect method to solve this problem, the description in analytical form is very complicated. Fortunately, the GPM provides an effective method to deal with the optimal problem with multiple constraints. The disadvantage of the GPM is that we have to increase the number of the discrete points, which reduces the computational speed. In order to overcome the above disadvantage, a *hp*–adaptive strategy [21], which obtains better performance by dividing the time interval into several subintervals, is widely used to reach the demand of solution precision and convergence speed. In order to facilitate the description of a mesh refinement method in the latter section, we firstly transform the trajectory optimization described as Eqs. (10)$\sim$(16) as the discrete bolza optimal control problem.

The time domain of the trajectory optimization problem is $[t_0, t_f]$. However, the discrete points of the Gauss pseudospectral methods are distributed in $[-1, +1]$. Thus, the time interval $t \in [t_0, t_f]$ is firstly transformed to the time interval $\tau \in [-1, +1]$. Assume that the time interval $\tau \in [-1, +1]$ is divided into a mesh comprising K mesh intervals $S_k = [T_{k-1}, T_k]$, where $-1 = T_0 < T_1 < \cdots T_k = +1$, $\bigcup_{k=1}^{K} S_k = [-1, +1]$, $k = 1, \ldots, K$. By introducing N_k Legendre-Gauss-Radau (LGR) collocation points, the continuous-time states $\mathbf{X}^{(k)}(\tau)$ and control inputs $\mathbf{u}^{(k)}(\tau)$ in S_k are approximated as $\bar{\mathbf{X}}^{(k)}(\tau)$ and $\bar{\mathbf{u}}^{(k)}(\tau)$, respectively. The trajectory optimization described as Eqs. (10)$\sim$(16) is rewritten as follows. Minimize the cost functional

$$J = \phi(\bar{\mathbf{X}}_1^{(1)}, t_0, \bar{\mathbf{X}}_{N_K+1}^{(K)}, t_f) = t_f \tag{17}$$

subject to the dynamic constraint

$$\sum_{j=1}^{N_k+1} D_{ij}^{(k)} \bar{\mathbf{X}}_j^{(k)} = \frac{t_f - t_0}{2} f(\bar{\mathbf{X}}_i^{(k)}, \bar{\mathbf{U}}_i^{(k)}, t(\tau_i^{(k)}, t_0, t_f)), \quad i = 1, \ldots, N_k \tag{18}$$

the path constraints

$$\mathbf{C}(\bar{\mathbf{X}}_i^{(k)}, \bar{\mathbf{U}}_i^{(k)}, t(\tau_i^{(k)}, t_0, t_f)) \le \mathbf{0}, \quad i = 1, \ldots, N_k \tag{19}$$

and the boundary condition

$$\boldsymbol{\psi}(\bar{\mathbf{X}}_1^{(1)}, t_0, \bar{\mathbf{X}}_{N_K+1}^{(K)}, t_f) = \mathbf{0} \tag{20}$$

where the path constraints consist of the constraints described as Eqs. (13)$\sim$(16) and the boundary condition is equivalent

to Eq. (12); $D_{ij}^{(k)}$ is the element of the $N_k \times (N_k+1)$ LGR differentiation matrix [38].

B. ALGORITHM FOR TRAJECTORY OPTMIZITION

In the previous section, the continuous-time trajectory optmizition problem has been discretized into a mesh M which consists of K mesh intervals $S_k = [T_{k-1}, T_k], k = 1, \ldots, K$, with N_k collocation points in each S_k. In order to meet the requriments of the accuracy tolerance, one solution is to set the number of the mesh intervals and the collocation points as much as possible. However, this solution will significantly increase the computation burden. Thus, the key problem is to design a mesh refinement method to meet the accuracy requriments with a small mesh scale.

Firstly, the solution relative error on current mesh M is estimated according to the approach in [27]. Assume that the number of the collocation points in the mesh interval S_k has increased, i.e., there are $M_k = N_k + 1$ LGR points $\left(\hat{\tau}_1^{(k)}, \ldots, \hat{\tau}_{M_k}^{(k)}\right)$ in S_k, where $\hat{\tau}_1^{(k)} = \tau_1^{(k)} = T_{k-1}$, $\hat{\tau}_{M_k}^{(k)} = T_k$. The relative error in the i^{th} component of the states is defined as

$$e_i^{(k)}\left(\hat{\tau}_l^{(k)}\right) = \frac{E_i^{(k)}\left(\hat{\tau}_l^{(k)}\right)}{1 + \max\limits_{j\in[1,\ldots,N_k+1],k\in[1,\ldots,K]}\left|\overline{X}_i^{(k)}\left(\tau_l^{(k)}\right)\right|}, \quad l = 1, \ldots, M_k+1, \quad i = 1, \ldots, n_x \tag{21}$$

with

$$E_i^{(k)}(\hat{\tau}_l^{(k)}) = \left|\hat{X}_i^{(k)}(\hat{\tau}_l^{(k)}) - \bar{X}_i^{(k)}(\hat{\tau}_l^{(k)})\right| \tag{22}$$

where n_x is the number of the states $\mathbf{X}^{(k)}(\tau)$.

The maximum relative error in S_k is defined as

$$e_{\max}^{(k)} = \max_{i\in[1,\ldots,n_x],l\in[1,\ldots,M_k+1]} e_i^{(k)}(\hat{\tau}_j^{(k)}) \tag{23}$$

Afterwards, the mesh refinement method is designed in the following two aspects: (i) $e_{\max}^{(k)} > \varepsilon$, (ii) $e_{\max}^{(k)} \le \varepsilon$,where ε denotes the mesh refinement accuracy tolerance which is set by user.

When the error tolerance is not satisfied, i.e., $e_{\max}^{(k)} > \varepsilon$, the relative error is reduced by dividing the mesh interval or increasing the number of collocation points in the mesh interval. If there are non-smooth points in the mesh interval S_k, the method of dividing the mesh interval is adopted; otherwise, the method of increasing the number of collocation points is used.

The non-smooth points are determined according to [29]. Assuming that there are H_i non-smooth points in S_k, the mesh interval S_k is divided into $H_k + 1$ subintervals. In order to avoid excessive mesh scales, the number of the subinterval is limited to $H_{\max}$. As a result, the number of the subinterval is determined by

$$S = \min(H_k + 1, H_{\max}) \tag{24}$$

If there are not non-smooth points in the mesh interval S_k, we improve the accuracy by increasing the number of collocation points. To satisfy $e_{\max}^{(k)} \le \varepsilon$, the relative error $e_{\max}^{(k)}$ should be multiplied by the factor $\varepsilon / e_{\max}^{(k)}$. The increase in the number of collocation points P_k is determined by [30]

$$P_k = \log_{N_k^{(M)}}\left(\frac{e_{\max}^{(k)}}{\varepsilon}\right) \tag{25}$$

Because the P_k defined by Eq. (25) may not be an integer, we have

$$N_k^{(M+1)} = \text{ceil}\left[N_k^{(M)} + \log_{N_k^{(M)}}\left(\frac{e_{\max}^{(k)}}{\varepsilon}\right)\right] \tag{26}$$

where ceil$[\cdot]$ denotes the argument with the next highest integer.

When the error tolerance is satisfied, i.e., $e_{\max}^{(k)} \le \varepsilon$, the mesh scale is reduced by reducing the number of collocation points in a mesh interval and merging adjacent mesh intervals. Let $\mu_k = (T_{k-1} + T_k)/2$, and $h_k = (T_k - T_{k-1})/2$ be the midpoint and half-width of the mesh interval, respectively. The i^{th} component of the state approximation is given as

$$X_i^{(k)}(\tau) = \sum_{j=1}^{N_k+1} X_{ij}\ell_j\left(\frac{\tau - \mu_k}{h_k}\right), \quad \ell_j(s) = \prod_{\substack{i=1\\ i\neq j}}^{N_k+1}\left(\frac{s - s_i}{s_j - s_i}\right) \tag{27}$$

where $-1 = s_1 < s_2 < \ldots < s_{N_k} < s_{N_k+1} = 1$ are the collocation points.

The polynomial $\ell_j(s)$ is rewritten as

$$\ell_j(s) = \sum_{l=0}^{N_k} a_{lj}s^l \tag{28}$$

where a_{lj} depends only on the collocation points.

Substituting (28) into (27), we have

$$X_i^{(k)}(\tau) = \sum_{l=0}^{N_k} b_{ij}\left(\frac{\tau - \mu_k}{h_k}\right)^l, \quad b_{ij} = \sum_{j=1}^{N_k+1} X_{ij}a_{ij} \tag{29}$$

The quantities which are difined to normalize the coefficients b_{ij} are given as

$$\beta_{ij} = 1 + \max_{k\in[1,\ldots,K]}\max_{\tau\in S_k}\left|X_i^{(k)}(\tau)\right|, \quad (i = 1, \ldots, n_x) \tag{30}$$

According to the difinition of μ_k and h_k, the ineqality $|\tau - \mu_k|/h_k \le 1$ holds for $\tau \in S_k$. if the N_k^{th} degree term in Eq. (29) is removed, the maximum relative error in S_k is $\left|b_{iN_k}\right|/\beta_{ij}$. All terms in Eq. (29) are removed from high degree to low degree until $\left|b_{ij}\right|/\beta_{ij} > \varepsilon$. For all components of the state $i \in [1, \ldots, n_x]$, the process mentioned above is repeated, resulting in the reduced polynomial degrees $\left(N_1^{(k)}, \ldots, N_{n_x}^{(k)}\right)$. The number of collocation points in S_k is selected as the maximun of $\left(N_1^{(k)}, \ldots, N_{n_x}^{(k)}\right)$.

As for merging adjacent mesh intervals, the conditions are given as follows: (i) two mesh intervals are adjacent, and

$N_{k+1} = N_k$; (ii) the relative errors of two mesh intervals are not greater than the error tolerance ε; (iii) the relative error of the merged mesh interval are not greater than ε.

The algorithm for solving the trajectory optimization problem is summarized as follows.

Step 1: Transform the trajectory optimization problem described as Eqs. (10)∼(16) into the bolza optimal control problem described as Eqs. (17)∼(20).

Step 2: Supply an initial mesh M comprising K mesh intervals $S_k = [T_{k-1}, T_k], k = 1, \ldots, K$, with N_k collocation points in S_k.

Step 3: Solve the bolza optimal control problem described as Eqs. (17)∼(20) using the NLP solver SNOPT in [39].

Step 4: The maximum relative error $e_{\max}^{(k)}$, $k = 1, \ldots, K$, on current mesh M is estimated using the Eq. (23).

Step 5: If the inequality $e_{\max}^{(k)} \leq \varepsilon$ holds for all $k = 1, \ldots, K$, then quit. Otherwise, proceed to Step 6.

Step 6: Get a refined mesh $M+1$. For every mesh intervals $S_k = [T_{k-1}, T_k]$, $k = 1, \ldots, K$, (a) if the error tolerance is not satisfied, i.e., $e_{\max}^{(k)} > \varepsilon$, divide the mesh interval (by Eq. (24)) or increase the number of collocation points(by Eq. (26)). (b) If the error tolerance is satisfied, i.e., $e_{\max}^{(k)} \leq \varepsilon$, reduce the number of collocation points and merge adjacent mesh intervals.

Step 7: Return to Step 3.

IV. SIMULATIONS

This Section implements a simulation study to verify the performance of the optimal maneuver trajectory proposed in this paper. The simulation is carried out in three aspects. Firstly, the performance of the improved *hp*-adaptive pseudospectral method proposed in this paper is verified, by comparing with the pseudospectral method in [27]. Secondly, an optimal maneuver trajectory is obtained by solving the designed trajectory optimization problem in Section II with the proposed algorithm in Section III. In order to verify that the trajectory obtained by the designed algorithm is in accordance with the actual flight law, Runge-Kutta method is used to solve the dynamic model described as Eqs. (1)∼(6) in which the value of the control input corresponds to the optimal trajectory. Finally, the effectiveness of the inverted flight is verified by comparing the results of normal flight and inverted flight.

A. RESSULTS OF MESH REFINEMENT METHOD

To test the performance of the mesh refinement method proposed in Section III, the hypersensitive optimal control problem [40] is considered. The objective is selected by minimizing the cost functional

$$J = \frac{1}{2}\int_0^{t_f} (x^2 + u^2)dt \tag{31}$$

subject to the dynamic constraint

$$\dot{x} = -x + u \tag{32}$$

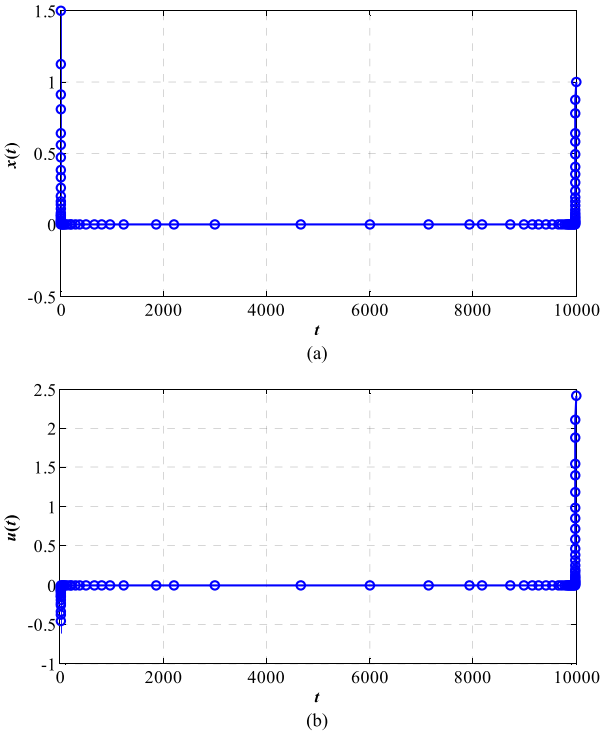

FIGURE 2. Exact solution to the hypersensitive problem with $t_f = 10000$. (a) State vs. Time. (b) Control vs. Time.

and the boundary conditions

$$x(0) = 1.5, \quad x(t_f) = 1 \tag{33}$$

where t_f is fixed.

The parameter M is the number of mesh refinement iterations, and $M = 0$ denotes the mesh initialization. The fixed terminal time t_f is selected as 10000 because the solution to the problem described as Eqs. (31)∼(33) exhibits a so-called take-off, cruise, and landing structure for a sufficiently large value of t_f. The initial mesh $M = 0$ consisting of 10 evenly distributed mesh intervals, with 2 collocation points in mesh interval. The error tolerance $\varepsilon = 10^{-6}$. The simulation results are depicted in Figs. (2)∼(3).

Fig. 2 shows the exact solution to the hypersensitive problem described as Eqs. (31)∼(33). It can be seen from Fig. 2 that the state and control change greatly near the ends of time, while the changing trend is relatively smooth in the middle of time. When using the collocation method to solve this hypersensitive problem, it can be concluded that more collocation points are needed near the ends of time, and the number of collocation points required in the middle of time is relatively smaller. The above characteristics of the solution are suitable for testing the effectiveness of the designed algorithm.

The mesh refinement history of the method in [27] is shown in Fig. 3(a), and the result of the method proposed in this paper is shown in Fig. 3(b). For this two methods, the results show that the collocation points are mainly ditributed near the ends of time, which is consistent with the exact

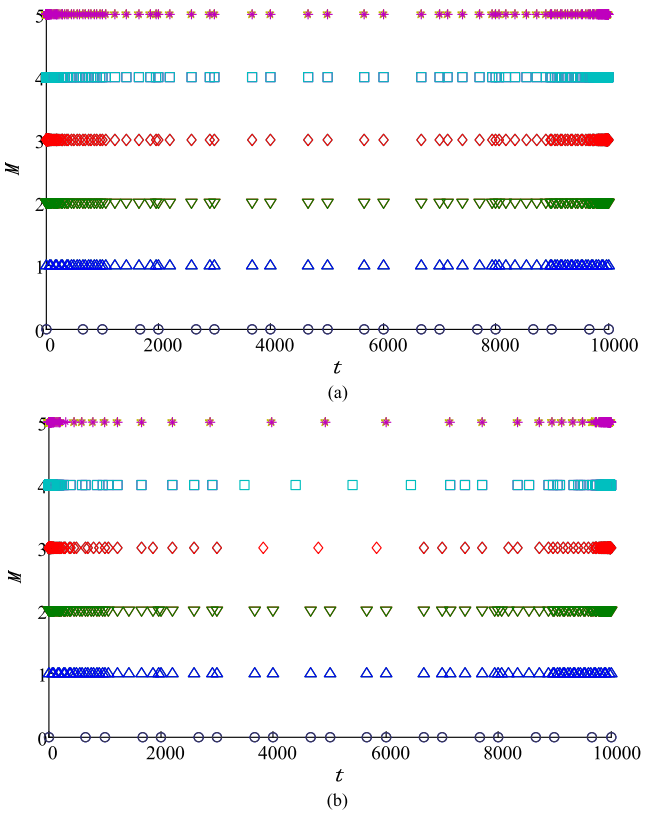

FIGURE 3. Mesh refinement history with the error tolerance $\varepsilon = 10^{-6}$. (a) Mesh refinement history by the method in [27]. (b) Mesh refinement history by the proposed method.

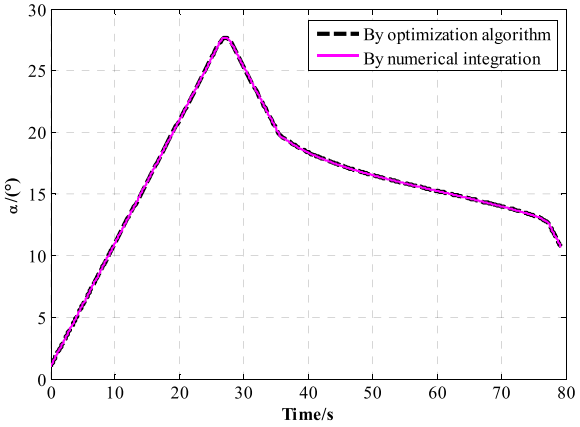

FIGURE 4. Curves of the angle of attack.

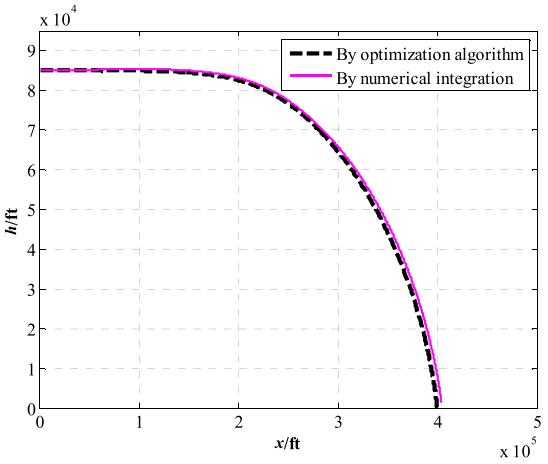

FIGURE 5. Curves of the trajectory.

solution in Fig. 2. In Fig. 3(a), the number of the collocation points increases as M increases. Different from the results in Fig. 3(a), it can be seen from the Fig. 3(b) that the number of the collocation points decreases as M increases when $M \geq 3$. The result in Fig. 3(b) indicates that the proposed mesh refinement method can significantly reduce the mesh scale with a satisfactory accuracy.

B. RESULTS OF OPTIMAL TRAJECTORY

The model parameters for hypersonic missile are selected according to [33], and the parameters for atmosphere model [34] are selected as $\rho_0 = 6.7429 \times 10^{-5}\text{slugs} \cdot \text{ft}^{-3}$, $h_0 = 85000\text{ft}$, $h_s = 21358\text{ft}$. The initial value of the states are given as follows: $x_0 = 0$, $h_0 = 85000\text{ft}$, $V_0 = 7700\text{ft/s}$, $\gamma_0 = 0$. The terminal state constraints are given by $x_f = 4 \times 10^5\text{ft}$, $h_f = 0$, $\gamma_f = -65^\text{o}$. The maximum values of the dynamic pressure, heating transfer rate, and normal overload are given as follows: $q_{\max} = 3.1315 \times 10^4\text{lbF/(ft}^2)$, $\{n_y\}_{\max} = 10$, $\{Q_{\text{rate}}\}_{\max} = 200BTU/(ft^2 \cdot s)$. The maneuvering form is selected as inverted flight.

Because the *hp*–adaptive Gauss pseudospectral methods obtain the approximation of states by the Gauss-Lobatto polynomial interpolation, rather than by the numerical integration, it is necessary to compare the results of optimization algorithm with the results of numerical integration. The control α of the optimal trajectory is taken as the input of the model differential equations described as Eqs. (1)∼(6), and the results of numerical integration are obtained by Runge-Kutta method. The simulation results are depicted in Figs. (4)∼(10).

Figs. (4)∼(7) show the curves of the angle of attack, trajectory, velocity, and flight path angle, respectively. The results by the proposed trajectory optimization algorithm are depicted as the dotted lines, and the results by numerical integration as the solid lines. By contrast, we can see that the results of the proposed trajectory optimization algorithm is consistent with those of numerical integration. it can be concluded that the proposed optimization algorithm can reflect the actual motion law of the hypersonic missile with a high accuracy. Moreover, the results indicates that the whole maneuvering trajectory is smooth.

Next, we analyze the characteristics of the trajectory obtained by the proposed trajectory optimization algorithm. As shown in Fig. (4), the control input, namely the angle of attack, is within a reasonable range ($\alpha \in (0, 30°)$). In Fig. (5), the optimal maneuver trajectory indicates that the hypersonic missile reaches the location of the target. It can be seen from Fig. (6) that the velocity is a downward trend, which is is

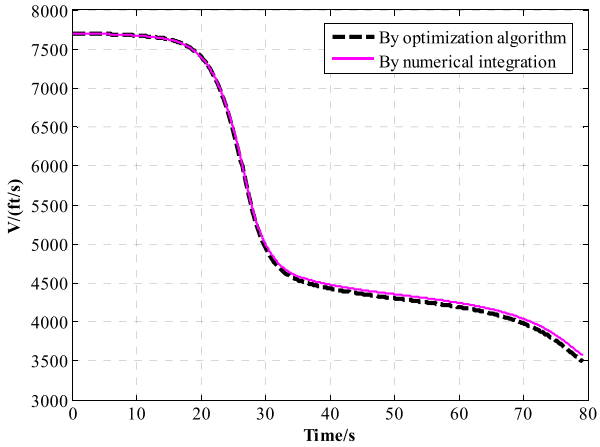

FIGURE 6. Curves of the velocity.

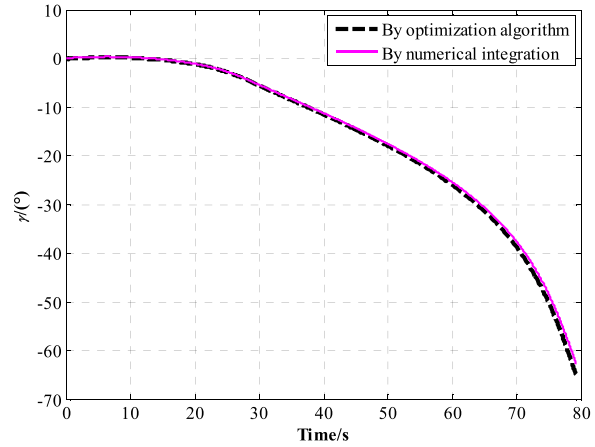

FIGURE 7. Curves of the flight path angle.

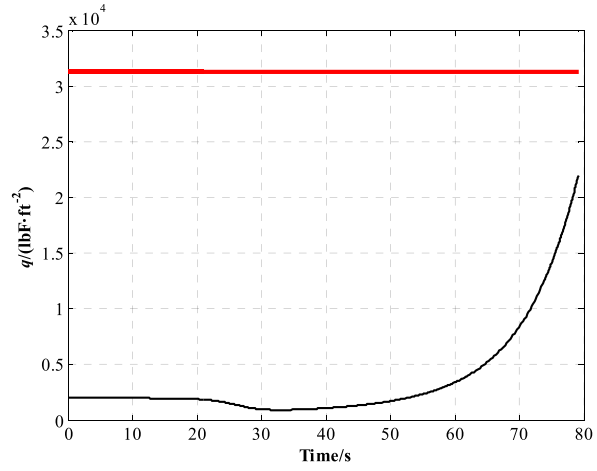

FIGURE 8. Curve of the dynamic pressure.

caused by the constraints of heating transfer rate and dynamic pressure. Fig. (7) shows that the terminal flight path angle achieves a preset value. Figs. (8)∼(10) show the curves of the dynamic pressure, heating transfer rate, and normal overload, respectively. The results reveal that the dynamic pressure,

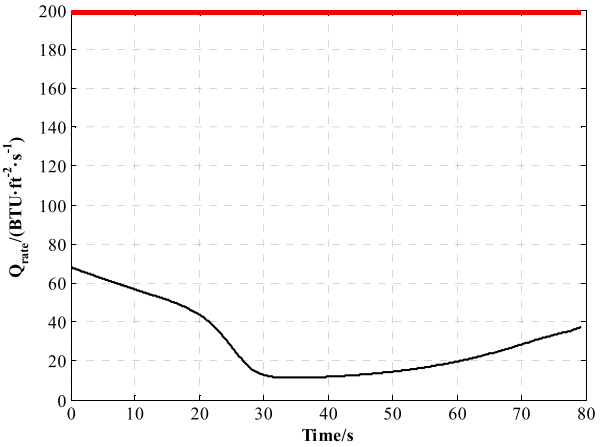

FIGURE 9. Curve of the heating transfer rate.

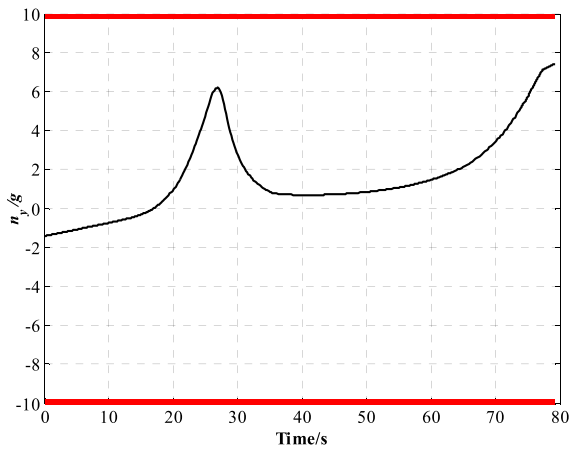

FIGURE 10. Curve of the normal overload.

TABLE 1. Maneuvering forms and terminal flight path angles.

Trajectory number	Maneuvering form	Constraint of terminal flight path angle
Tra 1	Normal flight	35°
Tra 2	Normal flight	50°
Tra 3	Normal flight	65°
Tra 4	Inverted flight	35°
Tra 5	Inverted flight	65°
Tra 6	Inverted flight	80°

heating transfer rate, and normal overload are within their constraints throughout the whole flight.

C. COMPARISON OF NORMAL FLIGHT AND INVERTED FLIGHT

To verify the effectiveness of inverted flight, the following simulation is carried out. The maneuvering form and terminal flight path angle are selected as Table 1, and other conditions are set to the same as those in the section B. The simulation results are given in Fig. (11)∼(12).

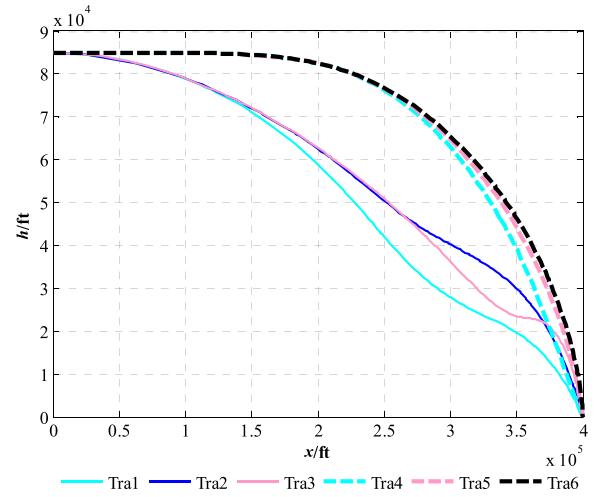

FIGURE 11. Curves of the trajectory.

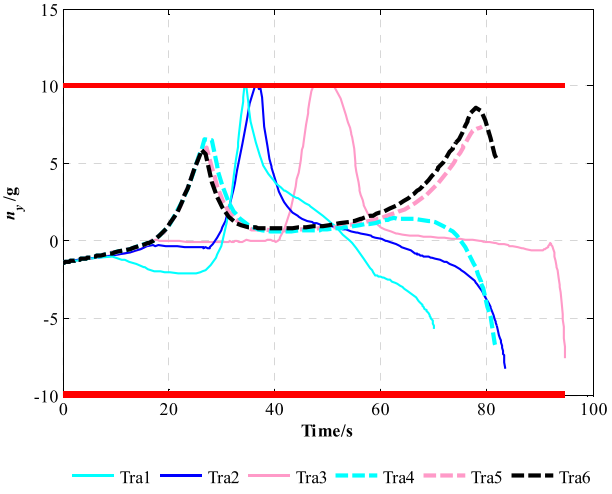

FIGURE 12. Curves of the normal overload.

Fig. (11) shows the trajectory curves of Tra 1∼Tra 6. It can be seen that the trajectory curve of the inverted flight has a shape of approximate parabola, and are smoother than that of normal flight. In the process of simulation, we found that it is relatively easy to obtain an optimal trajectory under a large terminal flight path angle by using inverted flight. However, a large preset terminal flight path angle under normal flight, with the same parameter settings, will cause the result to diverge.

The normal overload curves of Tra 1∼Tra 6 are given in Fig. (12). It can be seen that the normal overload curves of the normal flight are not satisfactory. The saturation time of normal overload becomes longer when the preset terminal flight path angle increases. Long saturation time of normal overload will increase the difficulty of controller design and even lead to the loss of control. In contrast, the normal overload curves of the inverted flight are always within the constraint, even when the preset terminal flight path angle is relatively larger. Thus, it can be concluded that the inverted flight has more advantages for the hypersonic missiles in dive phase. By contrast simulation, the effectiveness of the inverted flight is verified.

V. CONCLUSION

An optimal maneuver trajectory is presented for the hypersonic missiles in dive phase in this paper. Compared with previous studies, a maneuvering form named the inverted flight is first applied to the hypersonic missiles. Furthermore, an improved *hp*-adaptive pseudospectral method with mesh size reduction is designed to solve the trajectory optimization problem. Simulation results show that the proposed algorithm can significantly reduce the mesh scale with a satisfactory accuracy, and the effectiveness of the inverted flight is verified by comparative simulation. The work in this paper provides a maneuver strategy for the hypersonic missiles in dive phase to break through enemy's air defense system and maximize target penetration.

APPENDIX

The CFM [33] used in this paper is summarized in this section. The expressions of C_L, C_D and C_N are given as follows.

$$\begin{aligned} C_L &= \boldsymbol{C}_{L,Ma} \cdot \boldsymbol{M}_{a,L} + \mathbf{C}_{L,\alpha} \cdot \boldsymbol{\alpha}_L \\ &= \begin{bmatrix} -0.081929 \\ 0.0470142 \\ -0.00919 \\ 0.000774 \\ -0.0000293 \\ 0.000000412 \end{bmatrix}^T \begin{bmatrix} M_a^0 \\ M_a^1 \\ M_a^2 \\ M_a^3 \\ M_a^4 \\ M_a^5 \end{bmatrix} \\ &\quad + \begin{bmatrix} 1.07727 - 0.0265M_a \\ -0.49898 + 0.0019M_a^2 \\ 0.76741107 \\ -4.21373565 \\ 8.02706009 \end{bmatrix}^T \begin{bmatrix} \alpha \\ \alpha^2 \\ \alpha^3 \\ \alpha^4 \\ \alpha^5 \end{bmatrix} \end{aligned} \tag{34}$$

$$\begin{aligned} C_D &= \boldsymbol{C}_{D,Ma} \cdot \boldsymbol{M}_{a,D} + \boldsymbol{C}_{D,\alpha} \cdot \boldsymbol{\alpha}_D \\ &= \begin{bmatrix} 0.08883096 \\ -0.03339562 \\ 0.005044728 \\ -0.0003658 \\ 0.00001274 \\ -0.00000017 \end{bmatrix}^T \begin{bmatrix} M_a^0 \\ M_a^1 \\ M_a^2 \\ M_a^3 \\ M_a^4 \\ M_a^5 \end{bmatrix} \\ &\quad + \begin{bmatrix} 0.183 - 0.00716M_a \\ -3.587 + 0.0005M_a^2 \\ 59.71887625 \\ -321.68800332 \\ 603.01745298 \end{bmatrix}^T \begin{bmatrix} \alpha \\ \alpha^2 \\ \alpha^3 \\ \alpha^4 \\ \alpha^5 \end{bmatrix} \end{aligned} \tag{35}$$

$$\begin{aligned} C_N &= \boldsymbol{C}_{N,Ma} \cdot \boldsymbol{M}_{a,N} \cdot \beta + \boldsymbol{C}_{N,\alpha} \cdot \boldsymbol{\alpha}_N \cdot \beta \\ &= \begin{bmatrix} -0.29253 \\ 0.054822 \\ -0.0043203 \\ 0.00015495 \\ -0.0000020829 \end{bmatrix}^T \begin{bmatrix} M_a^1 \\ M_a^2 \\ M_a^3 \\ M_a^4 \\ M_a^5 \end{bmatrix} \beta \end{aligned}$$

$$+\begin{bmatrix} 0.16502903 - 0.01658312M_a \\ 2.41401 + 0.01516821M_a^2 \\ -70.3554194 \\ 303.723 - 0.2228107M_a^2 \\ -321.59490071 \end{bmatrix}^T \begin{bmatrix} \alpha \\ \alpha^2 \\ \alpha^3 \\ \alpha^4 \\ \alpha^5 \end{bmatrix} \beta \tag{36}$$

where α is the angle of attack, and β is the sideslip angle. M_a denotes the velocity of the hypersonic missile in Mach.

REFERENCES

[1] Y. Liu, B. Chen, Y. Li, and H. Shen, "Overview of control-centric integrated design for hypersonic vehicles," *Astrodynamics*, vol. 2, no. 4, pp. 307–324, 2018.
[2] D. Chai, Y.-W. Fang, Y.-L. Wu, and S.-H. Xu, "Boost-skipping trajectory optimization for air-breathing hypersonic missile," *Aerosp. Sci. Technol.*, vol. 46, pp. 506–513, Oct./Nov. 2015.
[3] X. Liu, W. Huang, and L. Du, "An integrated guidance and control approach in three-dimensional space for hypersonic missile constrained by impact angles," *ISA Trans.*, vol. 66, pp. 164–175, Jan. 2017.
[4] J. Li, C. Gao, C. Li, and W. Jing, "A survey on moving mass control technology," *Aerosp. Sci. Technol.*, vols. 82–83, pp. 594–606, Nov. 2018. doi: 10.1016/j.ast.2018.09.033.
[5] J. Li, S. Chen, C. Li, C. Gao, and W. Jing, "Adaptive control of underactuated flight vehicles with moving mass," *Aerosp. Sci. Technol.*, vol. 85, pp. 75–84, Feb. 2019.
[6] P. Yu, Y. Shtessel, and C. Edwards, "Continuous higher order sliding mode control with adaptation of air breathing hypersonic missile," *Int. J. Adapt. Control Signal Process.*, vol. 30, nos. 8–10, pp. 1099–1117, 2016. doi: 10.1002/acs.2664.
[7] M. V. Basin, P. Yu, and Y. B. Shtessel, "Hypersonic missile adaptive sliding mode control using finite- and fixed-time observers," *IEEE Trans. Ind. Electron.*, vol. 65, no. 1, pp. 930–941, Jan. 2018.
[8] S. Mehta, W. MacKunis, S. Subramanian, and C. Pasiliao, "Nonlinear control of hypersonic missiles for maximum target penetration," in *Proc. AIAA Guid., Navigat., Control Conf.*, Minneapolis, MN, USA, 2012, p. 4886.
[9] Y. Shtessel, P. Yu, S. S. Mehta, and C. L. Pasiliao, "Air breathing hypersonic missile continuous higher order sliding mode control for maximum target penetration," presented at the 13th IEEE Workshop Variable Struct. Syst. (VSS), Nantes, France, Jun./Jul. 2014.
[10] J. Zhu, L. Liu, G. Tang, and W. Bao, "Three-dimensional robust diving guidance for hypersonic vehicle," *Adv. Space Res.*, vol. 57, pp. 562–575, Jan. 2016.
[11] C.-S. Gao, J.-Q. Li, and W.-X. Jing, "A terminal guidance law based on motion camouflage strategy of air-to-ground missiles," *Int. J. Aerosp. Eng.*, vol. 2016, pp. 1–7, Aug. 2016.
[12] K. Sachan and R. Padhi, "A brief survey on six-degree-of-freedom modeling for air-breathing hypersonic vehicles," in *Proc. 5th IFAC Conf. Adv. Control Optim. Dyn. Syst. (ACODS)*, Hyderabad, India, 2018, pp. 492–497.
[13] J. Wang, L. Liu, T. Zhao, and G. Tang, "Integrated guidance and control for hypersonic vehicles in dive phase with multiple constraints," *Aerosp. Sci. Technol.*, vol. 53, pp. 103–115, Jun. 2016.
[14] C. Hongbo and L. Yongyuan, "Trajectory optimisation and analysis for hypersonic vehicle," *Int. J. Service Comput. Oriented Manuf.*, vol. 2, no. 2, pp. 179–188, 2016.
[15] G. N. Kumar, D. Penchalaiah, A. K. Sarkar, and S. E. Talole, "Hypersonic boost glide vehicle trajectory optimization using genetic algorithm," in *Proc. 5th IFAC Conf. Adv. Control Optim. Dyn. Syst. (ACODS)*, Hyderabad, India, 2018, pp. 118–123.
[16] C. Liao, M. Xu, X. Jia, and Y. Dong, "Semi-analytical acquisition algorithm for repeat-groundtrack orbit maintenance," *Astrodynamics*, vol. 2, no. 2, pp. 161–173, 2018.
[17] G. N. Kumar, M. Ikram, A. K. Sarkar, and S. E. Talole, "Hypersonic flight vehicle trajectory optimization using pattern search algorithm," *Optim. Eng.*, vol. 19, no. 1, pp. 125–161, 2018.
[18] H. Zhou, X. Wang, Y. Bai, and N. Cui, "Ascent phase trajectory optimization for vehicle with multi-combined cycle engine based on improved particle swarm optimization," *Acta Astron.*, vol. 140, pp. 156–165, Nov. 2017.
[19] H. Zhou, X. Wang, B. Bai, and N. Cui, "Reentry guidance with constrained impact for hypersonic weapon by novel particle swarm optimization," *Aerosp. Sci. Technol.*, vol. 78, pp. 205–213, Jul. 2018.
[20] S. Thabit and A. Mohades, "Multi-robot path planning based on multi-objective particle swarm optimization," *IEEE Access*, vol. 7, pp. 2138–2147, 2018.
[21] A. V. Rao *et al.*, "Algorithm 902: GPOPS, a MATLAB software for solving multiple-phase optimal control problems using the gauss pseudospectral method," *ACM Trans. Math. Softw.*, vol. 37, no. 2, pp. 22:1–22:39, 2010.
[22] Y. Mao, D. Zhang, and L. Wang, "Reentry trajectory optimization for hypersonic vehicle based on improved Gauss pseudospectral method," *Soft Comput.*, vol. 21, pp. 4583–4592, Jun. 2016.
[23] H. Lei, J. Zhou, D. Zhai, L. Shao, and D. Zhang, "Optimal midcourse trajectory cluster generation and trajectory modification for hypersonic interceptions," *J. Syst. Eng. Electron.*, vol. 28, no. 6, pp. 1162–1173, Dec. 2017.
[24] S. Yang, T. Cui, X. Hao, and D. Yu, "Trajectory optimization for a ramjet-powered vehicle in ascent phase via the Gauss pseudospectral method," *Aerosp. Sci. Technol.*, vol. 67, pp. 88–95, Aug. 2017.
[25] J. Zheng, J. Chang, S. Yang, X. Hao, and D. Yu, "Trajectory optimization for a TBCC-powered supersonic vehicle with transition thrust pinch," *Aerosp. Sci. Technol.*, vol. 84, pp. 214–222, Jan. 2019.
[26] J. Zhou, H. Lei, and D. Zhang, "Online optimal midcourse trajectory modification algorithm for hypersonic vehicle interceptions," *Aerosp. Sci. Technol.*, vol. 63, pp. 266–277, Apr. 2017. doi: 10.1016/j.ast.2016.12.022.
[27] M. A. Patterson, W. W. Hager, and A. V. Rao, "A *ph* mesh refinement method for optimal control," *Optim. Control Appl. Methods*, vol. 36, no. 4, pp. 398–421, 2015.
[28] M. Lin and M. Xu, "Entire flight trajectory design for temporary reconnaissance mission," *Trans. Jpn. Soc. Aeronaut. Space Sci.*, vol. 60, no. 3, pp. 137–151, 2017.
[29] F. Liu, W. W. Hager, and A. V. Rao, "Adaptive mesh refinement method for optimal control using decay rates of legendre polynomial coefficients," *IEEE Trans. Control Syst. Technol.*, vol. 26, no. 4, pp. 1475–1483, Jul. 2018.
[30] H. M. Lei, T. Liu, J. Li, and Z. P. Jiang, "Adaptive mesh refinement of hp pseudospectral method using size reduction," *Control Theory Appl.*, vol. 33, no. 8, pp. 1061–1067, Aug. 2016.
[31] J. D. Shaughnessy, S. Z. Pinckney, J. D. McMinn, C. I. Cruz, and M.-L. Kelley, "Hypersonic vehicle simulation model: Winged-cone configuration," NASA, Washington, DC, USA, Tech. Rep. TM-102610, 1990.
[32] J. Zhu, L. Liu, G. Tang, and W. Bao, "Optimal diving maneuver strategy considering guidance accuracy for hypersonic vehicle," *Acta Astronaut.*, vol. 104, pp. 231–242, Nov. 2014.
[33] J. Wang, L. Liu, P. Wang, and G. Tang, "Guidance and control system design for hypersonic vehicles in dive phase," *Aerosp. Sci. Technol.*, vol. 53, pp. 47–60, Jun. 2016.
[34] J. T. Parker, A. Serrani, S. Yurkovich, M. A. Bolender, and D. B. Doman, "Control-oriented modeling of an air-breathing hypersonic vehicle," *J. Guid., Control, Dyn.*, vol. 33, no. 3, pp. 856–869, 2007.
[35] S. Keshmiri, R. Colgren, and M. Mirmirani, "Six DoF nonlinear equations of motion for a generic hypersonic vehicle," in *Proc. AIAA Atmos. Flight Mech. Conf. Exhibit*, Hilton Head, SC, USA, 2007, p. 6626.
[36] R. Colgren, S. Keshmiri, and M. Mirmirani, "Nonlinear ten-degree-of-freedom dynamics model of a generic hypersonic vehicle," *J. Aircr.*, vol. 46, no. 3, pp. 800–813, May 2009.
[37] B. Tian, W. Fan, R. Su, and Q. Zong, "Real-time trajectory and attitude coordination control for reusable launch vehicle in reentry phase," *IEEE Trans. Ind. Electron.*, vol. 62, no. 3, pp. 1639–1650, Mar. 2015.
[38] D. Garg *et al.*, "Direct trajectory optimization and costate estimation of finite-horizon and infinite-horizon optimal control problems using a Radau pseudospectral method," *Comput. Optim. Appl.*, vol. 49, no. 2, pp. 335–358, 2011.
[39] P. E. Gill, W. Murray, and M. A. Saunders, "SNOPT: An SQP algorithm for large-scale constrained optimization," *SIAM Rev.*, vol. 47, no. 1, pp. 99–131, Jan. 2002.
[40] A. V. Rao and K. D. Mease, "Eigenvector approximate dichotomic basis method for solving hyper-sensitive optimal control problems," *Optim. Control Appl. Methods*, vol. 21, no. 1, pp. 1–19, 2000.

SHILI TAN was born in 1991. He received the B.S. degree in weapon system and launching engineering from Air Force Engineering University (AFEU), Xi'an, China, in 2014. He is currently pursuing the Ph.D. degree in control science and engineering from the Air and Missile Defense College, Air Force Engineering University. His research interests include modeling, trajectory optimization, and nonlinear control of hypersonic missiles.

HUMIN LEI was born in 1960. He received the M.S. and Ph.D. degrees in navigation guidance and control from the School of Astronautics, Northwestern Polytechnical University (NWPU), Xi'an, China, in 1989 and 1999, respectively. He was a Postdoctoral Fellow in control science and engineering from Xi'an Jiaotong University (XJTU). He is currently a Professor and a Supervisor for doctors with the Air and Missile Defense College, Air Force Engineering University (AFEU), Xi'an, China. He has authored two books and more than 150 articles, and holds three patents. His current research interests include advanced guidance law design, hypersonic vehicle controller design, and hypersonic interception strategy.

TAO LIU was born in 1988. He received the B.S., M.S., and Ph.D. degrees from Air Force Engineering University (AFEU), Xi'an, China, in 2011, 2013, and 2018, respectively. He is currently an Assistant Researcher with the China Aerodynamic Research and Development Centre (CARDC), Mianyang, China. His research interests include aerodynamic modeling for hypersonic missiles and the improvement of pseudospectral method.